CHALMERS UNIVERSITY OF TECHNOLOGY
Gothenburg, Sweden
www.chalmers.se

LICENTIATE THESIS

Paper is composed of wood fibers connected through mechanical interlocking and various microscopic forces. Modeling paper for paper product development requires that the microscopic fibers are resolved, as they are essential in papermaking. Wood type, composition, orientation are but a few parameters considered in paper development. However, modeling individual fibers leads to huge numerical problems on small scales due to paper's complex microstructure.

A simplified approach to paper modeling is presented and validated in this work. The proposed model sees the fibers as one-dimensional beams, modeled using classic linearized beam theory, resulting in a linear network model. This model was validated against experimental results for tensile stiffness, tensile strength, and bending resistance for several low-density paper sheets. These simulations are fast, only requiring a couple of minutes for each simulation.

Scaling the model leads to memory constraints on consumer hardware using a linear solver. Numerical upscaling, or homogenization, aims to simplify these large computations by solving smaller problems using efficient representations of the micro-structure instead of resolving all of the details. The numerical upscaling technique used and discussed in this work is the Local Orthogonal Decomposition (LOD) multi-scale method.

MORGAN GÖRTZ • Experimental validation and numerical upscaling of linear network models for simulation of paper • 2022

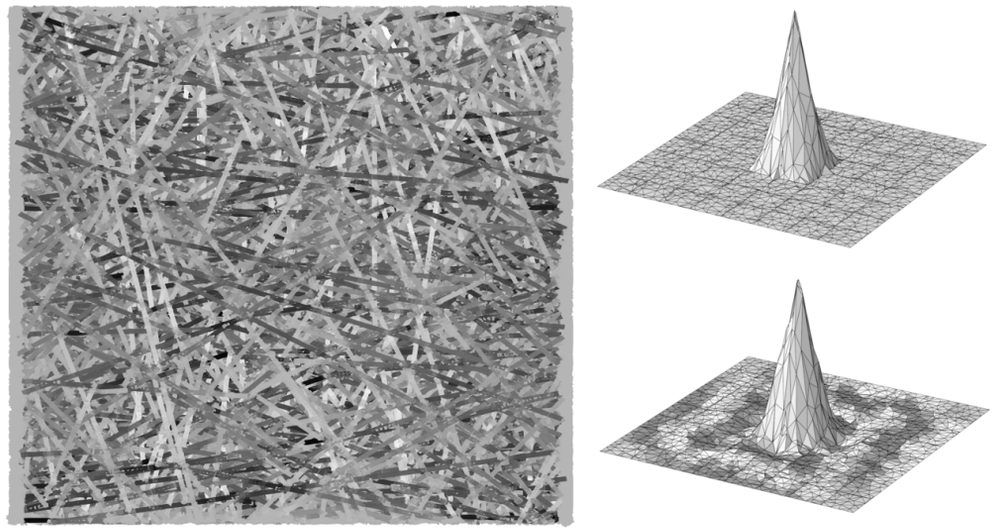

Experimental validation and numerical upscaling of linear network models for simulation of paper

MORGAN GÖRTZ

DEPARTMENT OF MATHEMATICAL SCIENCES
CHALMERS UNIVERSITY OF TECHNOLOGY
Gothenburg, Sweden 2022
www.chalmers.se

THESIS FOR THE DEGREE OF LICENTIATE OF PHILOSOPHY

Experimental validation and numerical upscaling of linear network models for simulation of paper

MORGAN GÖRTZ

Department of Mathematical Sciences
Chalmers University of Technology
Gothenburg, Sweden, 2022

Experimental validation and numerical upscaling of linear network models for simulation of paper

MORGAN GÖRTZ

Department of Mathematical Sciences
Chalmers University of Technology
SE-412 96 Gothenburg, Sweden
Phone: +46 (0)31 772 1000

Fraunhofer-Chalmers Research Centre for Industrial Mathematics
Department of Computational Engineering and Design
Chalmers Science Park
SE-412 88 Gothenburg, Sweden
Phone: +46 (0)31 309 9400
Email: morgan.gortz@fcc.chalmers.se

Printed by Chalmers Reproservice
Gothenburg, Sweden, 2022

Abstract

Paper modeling results in complex geometries that lead to enormous numerical problems. The complexity lies in the material's microstructure. Individual paper fibers must be considered for useful material simulations in paper development, where wood composition and other fiber-based parameters are essential. Multiple time-dependent and nonlinear modeling techniques have been proposed in the literature. In this work, a simplified approach to paper modeling is proposed. A simple but effective model can be created by seeing the paper as a network of one-dimensional beams and using linearized one-dimensional beam theory. Working in the industrial collaboration Innovative Simulation Of Paper (ISOP), the model was constructed to be relevant for paper developers, which means fast evaluations and representative results. The model was validated against experimental data for tensile stiffness, tensile strength, and bending resistance in both cross and machine direction for several low-density sheets. These simulations are fast, taking no more than a couple of minutes to generate and evaluate randomly generated paper samples.

For larger simulations, a multiscale approach is proposed. The multiscale method proposed is the LOD method, a generalized finite element method. In this method, the heterogeneities (fibers) in the paper model are resolved using special local orthogonal projection operators. This work presents the theoretical foundation of using the LOD method on discrete network models, which builds up to an a priori error bound for the multiscale approximations. The theoretical a priori error results are confirmed with numerical examples. Both structural problems and scalar-valued discrete network problems are presented in these examples. This work ends with numerical results showing the successful use of the LOD method on one of the structural simulations in the validation of the paper model, showing that the LOD method can be used for non-trivial simulations.

Keywords: Bending, local orthogonal decomposition, multiscale, network model, paper model, paper simulation.

List of Papers

This thesis is based on the following publications:

[A] **Morgan Görtz**, Gustav Kettil, Axel Målqvist, Andreas Mark, Fredrik Edelvik, "A numerical multiscale method for fiber networks". WCCM-ECCOMAS 2020.

[B] **Morgan Görtz**, Gustav Kettil, Axel Målqvist, Mats Fredlund, Kenneth Wester, Fredrik Edelvik, "Network models for predicting structural properties of paper". Submitted to: Nordic Pulp and Paper Research Journal.

[C] Fredrik Edelvik, Morgan Görtz, Fredrik Hellman, Gustav Kettil, Axel Målqvist, "Numerical homogenization of spatial network models". Numerical homogenization of spatial network models.

Contributions of the author

[A] Görtz developed and implemented the discrete LOD method, implemented compatible versions of the models for the LOD method, performed the numerical examples, and wrote the manuscript.

[B] Görtz developed large parts of the implementation of the paper model, researched and analyzed the parameters in the model, performed all of the numerical experiments, and wrote the manuscript.

[C] Görtz worked with the initial theoretical development, supported the theoretical development with numerical insights, implemented and performed the numerical examples in the article, and helped write the manuscript.

Acknowledgments

I want to thank the Swedish Foundation for Strategic Research (SSF) for supporting my research financially. Moreover, parts of this work have been done within the ISOP (Innovative Simulation Of Paper) project, and I would like to thank all the parties involved.

My supervisors: Axel Målqvist, Fredrik Edelvik, and Gustav Kettil, have all helped me greatly, and their help has been greatly appreciated. Axel Målqvist is always fun to talk to and has excellent idéas for new projects and how to tackle particular problems. Fredrik Edelvik has an eye for details, and his feedback on presentations and written work has been invaluable. Gustav Kettil helped me get started with the code and system at the research center and has been a person I can turn to for discussions regarding implementation.

Finally, I want to thank my close friends and family for their emotional support.

Contents

CHAPTER 1

Introduction

Paper has been around for a long time. At its core, a sheet of paper is composed of paper fibers meshed together through mechanical interlocking and microscopic forces [1]. The paper's properties depend on the manufacturing processes, but also wood species, tree age, and other material properties.

From wood to a sheet of paper, there are several steps. First, typically the wood is processed (mechanical or chemical) to separate the cellulose fibers. This process produces a fibrous material called pulp and the process pulping. After pulping, the pulp is refined and mechanically treated. With the raw material treated, the pulp is mixed in water and potential additives to produce what is known as a stock. This stock then goes in a paper machine, where the liquid is sprayed onto a forming fabric, creating paper. This paper is then typically processed further, such as drying and pressing.

The papermaking process involves many steps, with each step introducing some functionality in the paper produced. With modern papermaking machines requiring increasing amounts of energy and faster computers getting accessible, simulations of papermaking processes are getting realistic and preferable. A papermaker could check hypotheses on a computer before making prototypes, thus creating more educated trial runs. Moreover, simulations produce detailed results, and information

about the microscopic components in their papers can gain insights for future development.

Several groups have worked with simulating parts of the papermaking process, and properties of paper [2]–[4]. The Innovative Simulation Of Paper (ISOP) project is an industrial research project performed by a consortium consisting of Albany International, Stora Enso, and Fraunhofer-Chalmers Centre. This project aims to produce validated and actively used simulation tools in the product development of paper-based products. Within the project, tools for both forming simulations of paper [5] and edge wicking (fluid absorption) [6] have been developed. The paper model presented and validated in this book was performed within this project. The companies have played a vital role in this model's development by producing experimental data for mechanical properties, experimental data for the fibers used, and input on important features that the model should capture.

Simulating paper is challenging because of the material's complex microstructure. For an effective model in papermaking, the individual paper fibers need to be represented. The paper fibers play a vital role in the end product's properties. A simplified approach to paper simulation is presented in this work, where the individual paper fibers are edges in a network. Using a network model means that the geometries of the individual paper fibers are one-dimensional. However, cross-sectional information about the fibers is used and added analytically. The resulting paper model has been validated and can reproduce several structural experiments through simulation. These are tensile stiffness, tensile strength, and bending resistance. Moreover, paper has different structural properties depending on orientation (similar to wood, wood grain) because of the manufacturing process, and the model can represent these differences for the experiments mentioned. These simulations are fast and accessible for a papermaker, taking a couple of minutes to generate random paper models and perform the simulations.

Even though the simulations are fast, they scale poorly. Paper simulations produce representative results on small scales [7], which is good because of its complex microstructure. Larger simulations are bottlenecked by memory or computational complexity. However, larger simulations are still interesting, and in this work, a method that resolves these computational complexities is presented.

The method proposed for analyzing large paper models is a multiscale method that separates the problem into different scales. By only analyzing the details of the paper model in small areas, the method trades one enormous problem to multiple smaller ones. This process is known as homogenization or upscaling. Several

network problems have been upscaled, for example, heat conductivity in network models [8], traffic [9], and flow in porous media [10].

There are several multiscale methods for solving partial differential equations with rapid coefficients. Two of them are the Heterogeneous Multiscale Method (HMM) [11] and the Multiscale Finite Element Method (MsFEM) [12]. The multiscale method chosen for the paper model is the Local Orthogonal Decomposition (LOD) method [13]. This method can handle problems that are not periodic or scale separable. Moreover, elasticity problems have been analyzed with this method [14], [15], and initial numerical work in [16] showed that a discrete LOD method could handle models similar to the proposed paper network model.

This thesis presents the paper network model, how the individual fibers are modeled bonded together, and presents the governing model for evaluating its structural properties. With the model presented, several structural simulations are performed, presented, and validated against experimental data. This validation provides numerical metrics of the simulations, illustrating that a different approach is required for larger simulations. The proposed LOD method in this work is then presented, alongside theoretical work motivating the method's use on discrete network models. Numerical examples illustrate these theoretical results, and the book ends with one of the validation simulations being performed with the LOD method successfully.

CHAPTER 2

Paper Network Model

Paper on a microscopic scale looks like a network of interconnected paper fibers. The sheer amount of fibers in a sheet of paper makes representative models inherently complex, with models no larger than one square centimeter typically considered [3], [17]. However, these small domains can be sufficient. In [7], it was observed that 1.2 times the longest fiber in the composite material produced representative results for tensile simulations and two times the longest fiber for strength simulations. These findings are consistent with the domain analysis performed in **Article B** for tensile stiffness, strength, and bending resistance simulations for low-density paper models. Although the simulations are on small domains, the computations are non-trivial. In one approach, a 0.5×0.5 mm tensile simulation of a low-density paper required 6 hours to evaluate [3]. This chapter aims to present a simplified paper model, where each paper fiber is a one-dimensional line, and the cross-section information of each fiber is incorporated analytically.

2.1 Approach

In [18] a network model is presented, where the edges in the network represent the paper fibers, and the nodes are discretization points. The model, a generalization of

the finite difference discretization of the linear elasticity equation, is presented and expanded on in this chapter. These additions include adding cross-section information to all the fibers, making structural properties and bonding more accurate, and motivating the different parameters in the model using either experimental results or published values.

The model considered is simpler than many other approaches in the literature ([2], [3]). These simplifications allow for faster computations and evaluations. However, simplifications have to be motivated. Working with papermaking companies in the industrial research consortium Innovative Simulation of Paper (ISOP) has been a great asset with their input on essential properties and functionality in a paper model. ISOP is performed by a consortium consisting of Albany International, Stora Enso, and Fraunhofer-Chalmers Center, with the end goal being validated and actively used simulation tools in the product development of paper-based products.

The network model consists of geometric and mathematical representations to create a realistic and efficient paper model. Each fiber is modeled and given an initial relaxed position, and every paper model consists of a composition of these fibers. The paper fibers connect through bonds to create a cohesive material. Like real paper, only fibers close to each other will bond. The model allows separate structural properties in bonds and fibers. The network model's geometry is generated by placing the fibers in a domain and connecting them. With this geometry, structural-mechanical relations are applied mathematically to analyze the model's structural properties. In this chapter, the four parts of the model are presented in succession: the fiber model, fiber bonding, fiber placement, and lastly, the governing model used to evaluate the model's structural properties.

2.2 Paper fiber representation

Each fiber in the network model is modeled individually. The fiber model's geometry consists of several straight line segments representing the fiber's centerline. These line segments are the edges in the network model, where the points between the edges are the nodes. These nodes are where the fiber may bend. Because the edges can not bend, the fiber model's dynamic movement and shape depend on the number of edges. However, increasing the number of edges representing each fiber will increase the entire paper model's complexity. A proposed length of the edges is 0.1 mm, giving a 1 mm long fiber about 10 equally spaced nodes where the fiber can be shaped and bent. For a geometric representation, see Figure 2.1.

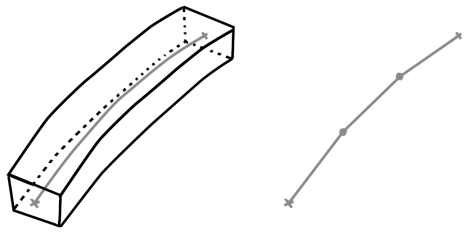

Figure 2.1: Illustration of the fiber model. The left figure shows a section of fiber with its centerline, and the right shows the fiber model representation with straight lines(edges).

Each edge in the paper model has information about its cross-section. The cross-section information includes fiber shape, cross-section area, fiber width, and cell wall thickness. These properties play an essential role in bonding, where the volumes of the edges are analyzed. Moreover, in evaluating structural properties of the edge, cross-section area is used for calculations of tensile strains, and the geometry defines the second moment of areas for bending related forces. An illustration of the parameters defining the cross-section of each edge is presented in Figure 2.2.

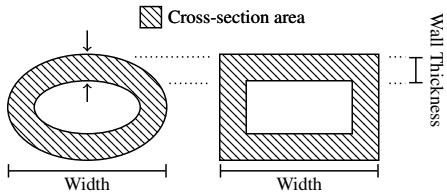

Figure 2.2: Cross section parameters for an elliptic shape and rectangular shape. Cross section area defines the total area of the cross section, width the width of the fiber, and cell wall thickness the thickness of the fiber walls.

2.3 Fiber bonding

Bonds connect the fibers in the network model. In the network model, bonding occurs if two fibers intersect based on the fibers' center lines and cross-sectional information. The bonding algorithm utilizes an R-tree for efficiency to find relevant segments that may intersect in the model based on the associated edges' midpoints. Intersections are found by triangularizing these three-dimensional fiber segments us-

ing the edges and their cross-section information and performing a geometric analysis. If two fiber segments intersect, the bond is placed based on the two points on the edges closest to each other. An illustration of the intersection process is provided in Figure 2.3.

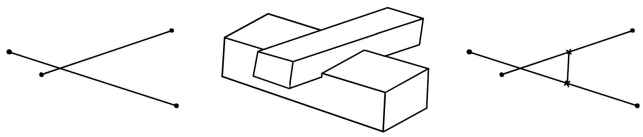

Figure 2.3: Illustration of the bonding process.

There are several ways to represent the individual bonds in a network model, and in finding an ideal approach, several bonds were analyzed. The first and most straightforward approach used is node-based bonding. Here a node is created between the two closest points between the segments to be bonded, and detour the segments to this common node (see Figure 2.4).

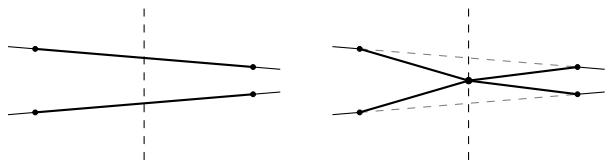

Figure 2.4: Illustration of the node bond. The left figure shows the two fibers segments before getting bonded, the right the resulting node bond.

Node bonds can successfully model tensile properties compared to validation data, but locking is observed for bending resistance simulations. Moreover, breaking a bond requires one of the fibers to break, which is not ideal. Instead, edge-based bonds can be used. For edge-based bonds, an edge is placed between the two closest nodes of the fiber segments. This edge is modeled as a fiber segment with structural properties similar to a fiber segment. An illustration of such an edge bond is presented in Figure 2.5.

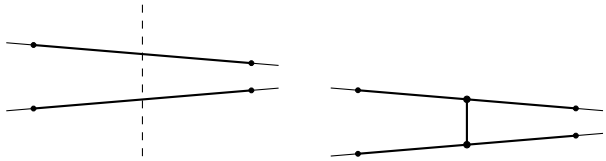

Figure 2.5: Illustration of the edge bond. The left figure shows the two fibers segments before getting bonded, the right the resulting edge bond.

The edge bond approach allows bonds to break, but locking is still observed. However, removing bending resistance in one plane removes the locking. With this restriction, these edge bonds are unable to model torsion if only one edge bond is present in a bond. This problem can be solved by adding multiple edge bonds per intersection and is the bonding technique that produces the best results. The amount of bonds created per intersection is defined as a discretization parameter, bond delta, and can be seen as the amount of refinement allowed of a fiber segment around a bond. The bonds' structural properties are weighted with bond delta to remove the structural effects of adding more bonds. The algorithm that places these edge bonds starts as before, with the closest pair of nodes in the two intersecting fiber segments. Then moving along each fiber in both directions by this discretization parameter, additional bonds are placed if the associated subvolumes intersect as well. An illustration of such an edge bond is presented in Figure 2.6

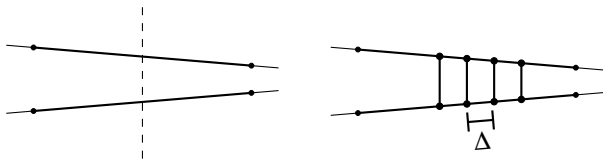

Figure 2.6: Illustration of the edge bond with multiple bonds with discretization parameter Δ. The left figure shows the two fibers segments before getting bonded, the right the resulting bond.

2.4 Network model generation

The paper forming process consists of paper fibers suspended in water pushed onto a forming fabric to create the fibrous material. The resulting sheet of paper depends on the machine used, its settings, the fiber mixture used in the process, and

the post-processing steps such as pressing involved. With so many variables, the model's parameters are categorized into three categories: macro-scale, micro-scale, and structural.

Macro-scale parameters are attributes that describe the properties of the paper sheet rather than the individual fibers. First, the paper **sheet size** gives a starting point for the model. The sheet's size gives the total area of the paper model, and a given **grammage** (weight per square meter) gives the total weight of all the paper fibers in the model. The paper fibers are placed somewhere in the domain specified by the sheet size. This placement may be determined by simulating the forming process as in [5], or through randomization given a **fixed thickness**. In either case, the fibers are typically oriented more in one direction (machine direction) than the other (cross direction), and this bias is introduced using a specified **fiber orientation distribution**.

Micro-scale parameters describe the properties of the individual paper fibers. Fibers generated in the modeling process have an initial position and orientation. However, each fiber may vary in **length** and **width**, and different wood types might be present in composites. In the generation process, wood type is randomly decided based on **wood composition**. A random fiber is generated using distributions for the specified wood type. The length of the fiber times the **coarseness** (weight per meter) of the wood defines the weight of the fiber.

The last parameters are called structural. These parameters are harder to measure and require more in-depth analysis to attain. These are **cross section area**, **cell wall thickness**, **Young's modulus**, and **fiber strength**. These parameters may be chosen from research results on individual fiber analysis [19]–[21] and can be dependent on wood type, fiber length, or other micro-scale properties. A detailed approach to generate the cross-section parameters and data on their dependence on other microscopic parameters can be found in [22].

2.5 Governing model

A linear system models the structural-mechanical properties of the network model. The system is formulated as:

$$Ku = F,\ u = [u_1, u_2, \ldots, u_n]^T,\ F = [F_1, F_2, \ldots, F_n]^T, \tag{2.1}$$

where n is the number of network nodes, $K \in \mathbb{R}^{3n\times 3n}$ is a connectivity matrix, $u_i = [u_{i,x}, u_{i,y}, u_{i,z}]$ are the three-directional nodal displacements, and $F_i = [F_{i,x}, F_{i,y}, F_{i,z}]$ are the applied forces in the i:th network node. The connectivity matrix, K, is composed of three linear force-displacement relations: edge extension, angular deviation and Poisson effect.

Edge extension defines the forces arising with the changes of the edges' lengths. These changes are quantified by their strains $\varepsilon = \frac{\Delta L}{L}$, where L is the initial length of an edge and ΔL is its change. The strains used in the model are linearized by using orthogonal projections (see Figure 2.7). Using the projected strain in the definition of Young's modulus, the magnitude of the resulting force in the model is:

$$E_A = \frac{\sigma}{\varepsilon} = \frac{F \cdot L}{A \cdot \Delta L} \Leftrightarrow F = \frac{E_A \cdot A \cdot \Delta L}{L}, \tag{2.2}$$

where E_A is the axial stiffness (Young's modulus), A is the cross-section area, and F is the quantified force arising from the displacement. These forces' directions are chosen to be parallel to the edges initial axes, again for linearity. An illustration of the forces arising from a displaced edge by edge extension can be seen in Figure 2.7.

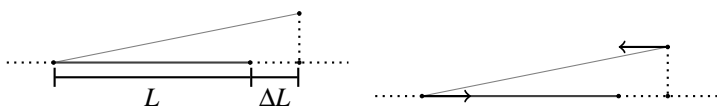

Figure 2.7: The thick lines are the initial edges and the thin lines are their displacements. The left figure shows how the difference in length is calculated by projecting the displaced nodes onto the fibers initial axis and the right shows the forces arising from the displacement.

Angular Deviation provides a counterforce when the angle between two connected edges is changed. This angular change is evaluated in two planes, one plane containing the pair of edges (in-plane) and the other orthogonal to the first (out of plane). Normal vectors to the edges in each of the planes are used in the angular deviation calculations (see Figure 2.8).

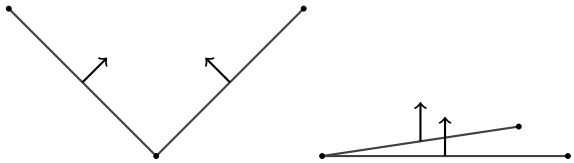

Figure 2.8: The normal vectors used in the two angular deviation equations. The left picture shows the normal vectors in the plane and the right shows the normal vectors out of the plane.

It is possible to approximate the angular change between the two edges in the edge pair using the aforementioned normal vectors. In this section, only the in-plane case is presented as the out of plane equations are analogous. Using the normal distance ΔL_1 in Figure 2.9, the angle $\delta\theta_1$ is approximated using:

$$\delta\theta_1 \approx \tan(\delta\theta_1) \approx \frac{\Delta L_1}{L_1},$$

assuming the displacement is small. Doing the same for the other edge gives an approximation for $\delta\theta_2$. These angles summed approximates the total angular change:

$$\Delta\theta = \delta\theta_1 + \delta\theta_2.$$

With this total angular change, the second derivative of the displacement in the normal direction of the center node can be approximated by:

$$u'' \approx \frac{\Delta\theta}{0.5(L_1 + L_2)},$$

as it coincides with the second order central finite difference scheme for straight edge pairs. Using Euler-Bernoulli beam theory, we have the following deformation/moment relation:

$$E_B \cdot I \cdot u'' = -M,$$

where E_B is the bending stiffness (Young's modulus), and I is the second moment of area. This second moment of area depends on the edges' cross-section geometry. Evaluating and expanding the moments in the central node gives the amplitude of the

angular deviation forces:

$$F_i = -\frac{E_B \cdot I}{L_i} u'' \approx -\frac{E_B \cdot I}{L_i} \left(\frac{\Delta\theta}{0.5(L_1 + L_2)} \right), \; i = 1, 2. \tag{2.3}$$

The forces are placed in each edge node with directions parallel to the normal vectors used to calculate the angular change. An illustration of these directional forces is provided in Figure 2.9.

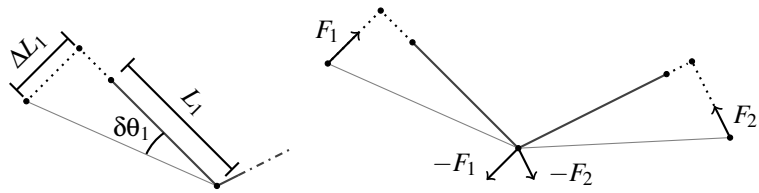

Figure 2.9: The thick lines are the initial edges and the thin lines are their displacements. The left figure shows the geometrical relation between L_1, ΔL_1, and $\delta\theta_1$. The right figure shows the forces arising from the angular deviation equation given a displacement.

Poisson Effect is a force displacement relations that is added to make specific networks equivalent to a finite difference discretization of the linear elasticity equations. The finite difference networks do not represent beams, but rather some level of homogenization. To read more about the Poisson effect and the different non-fiber based network models, see [18].

CHAPTER 3

Mechanical Simulation of Paper

With the model presented in Chapter 2 several structural simulations are possible. This chapter presents three different types of simulations: tensile stiffness, tensile strength, and bending resistance. Experiments performed by Albany International and Stora Enso are used to validate these simulations in both machine and cross direction.

3.1 Mechanical tests

The mechanical simulations considered try to replicate experiments used in paper development. Paper has several key properties that papermakers keep in mind in paper development. These include the three types analyzed in this work: tensile stiffness, tensile strength, and bending resistance.

The tensile properties of the paper analyzed here are tensile strength and tensile stiffness. A paper sample is placed in an apparatus that clamp two opposite sides of the sheet in the experiment. The sheet is then strained progressively, with the forces required to hold the strains measured simultaneously. This progression continues until the sample breaks. Tensile stiffness is evaluated as the amount of force required to strain the paper for elastic deformations, and tensile strength is the total force

required to break the sample.

Square models are used in the simulation of the tensile experiments. These square models are divided into three domains as in Figure 3.1, with two thin domains along two opposite sides that represent the paper parts being fixed into place by the tensile test equipment. One domain is fixed and can not move, and the other is displaced to some specified strain. Similar to the experiment, the strain is marginally increased in each iteration, with fibers stretched above their breaking point removed to emulate breakage. This iteration is continued until the force required to strain the model drops below 70% of the highest force observed, at which point the paper is assumed to be structurally compromised.

For tensile stiffness simulations, the strain is set far below the breaking point, and the stiffness is calculated based on the force required to achieve the specified strain using the following formula:

$$\text{Tensile Stiffness} = \frac{F}{\text{Width} \cdot \text{Strain}},$$

whereas, tensile strength simulations are performed until breakage and calculated by the following formula:

$$\text{Tensile Strength} = \frac{F_{\max}}{\text{Width}}.$$

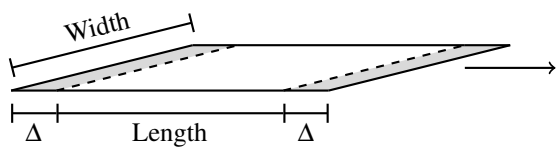

Figure 3.1: Tensile test geometry. Gray areas are clamped and pulled (arrow) to strain the white zone of the model.

In a bending resistance experiment, the force of bending a sheet of paper is evaluated given specific leverage and angle. A paper sample is fixed at one end and then bent, with the leverage, to the specified degree. A measuring probe does the pushing and measures the force simultaneously. The normalized force with respect to the width of the paper required to push the paper is considered the bending resistance.

The bending resistance simulation is performed on rectangular paper models, with the paper sample's length (leverage) being the same as in the experiment. This sim-

ulation fixes the paper model on one side, again similar to the tensile setup, and displaces the model at the specified leverage to the given angle. An illustration of this setup is presented in Figure 3.2. Unlike the tensile simulations, this bending simulation is slightly different from its experimental counterpart. In the bending resistance experiments, the measurement probe that bends the sheet can move along the sheet, whereas it does not move in the simulation. This simplification is motivated by the effect of the small movements is assumed to be negligible. Slight modifications to the model are made in the bending resistance simulations. The displacement occurs in a slim domain, so extra nodes are placed on edges passing through this area. With this slight modification, the bending resistance with leverage and angle θ is calculated by:

$$\text{Bending Resistance} = \frac{F_z \cos(\theta) + F_x \sin(\theta)}{\text{Width}},$$

where F_x, and F_y are the directional components of the force observed in the simulation.

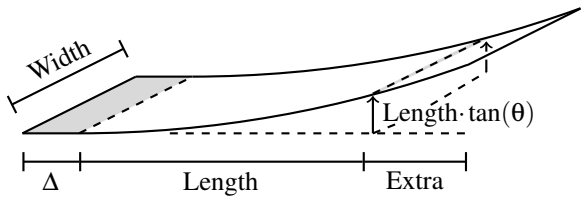

Figure 3.2: Bending test geometry. Gray area to the left is clamped and the right dashed line is displaced (arrows) given a bending angle θ.

3.2 Model Validation

The network model needs to be validated to be justified. The validation compares simulated results to experimental results achieved during two separate experimental runs performed at Stora Enso years apart. The first experimental run analyzed the structural properties of sheets generated in a pilot paper machine at The Packaging Greenhouse in 2012. For the second experimental run, sheets were generated at Albany International in 2020. The same parameter setup will be used for both experiments, with the macro-level parameters defining the simulation parameters for the different experiments.

The parameters used in the model for the following validation are given by ex-

perimental or published values. The macro-level parameters **grammage** and **thickness** are measured for each sample in the experiments, with **sheet size** being chosen based of domain studies, and **fiber orientation** from the work performed in [23]. Micro-scale parameters are generated using fiber distribution data from an analysis performed on one of the pulp mixtures used in the experiments. The structural parameters are chosen from literature [19]–[21], [24]. The fibers in the model are placed at random, cyclicly, with uniform coverage given a measured thickness for each sample. Laydown simulations [5] were not used for efficiency. For a more in-depth discussion of the choice of the parameters, and the domain study, see **Article B**.

The Packaging Greenhouse experiments, 2012

In the packaging greenhouse experiments: tensile stiffness, tensile strength, and bending resistance, among others, were measured for an assortment of low-density samples. The low-density samples were produced over three days on a pilot board machine in a standard configuration. Of the resulting samples, fourteen are used in this validation with grammages between 30 and 60 g/m^2. The three structural properties of these samples, in machine and cross direction, were tested at Stora Enso and lay the foundation for the validation data in **Paper B**.

The three experimental setups: tensile stiffness, tensile strength, and bending resistance, are modeled using the setups presented. In the tensile simulations, 4 mm square paper models were used to evaluate the model's properties, whereas a 4×11 mm model was used for the bending resistance simulations with leverage 10mm and angle 15 degrees. Both machine direction and cross direction were simulated and compared for each experimental result.

For the simulations to be relevant, the models need to move appropriately and produce validated results. The tensile strains in a tensile simulation, a fault line from a strength simulation, and a bending curve are presented. In Figure 3.3 both extended and compressed fibers are visible in a tensile stiffness simulation along with a nontrivial fault line in a tensile strength simulation. A bending profile is presented in Figure 3.4 to illustrate how the model acts in the bending resistance simulation. In all cases, it is clear that the model moves as one would expect.

Ten samples were evaluated for each sample in the experiment, in both machine and cross direction, and the mean and standard deviation of the runs are the presented results. The same procedure was performed in the simulations, generating ten random models for each sample. The validation results are presented in Figure 3.5.

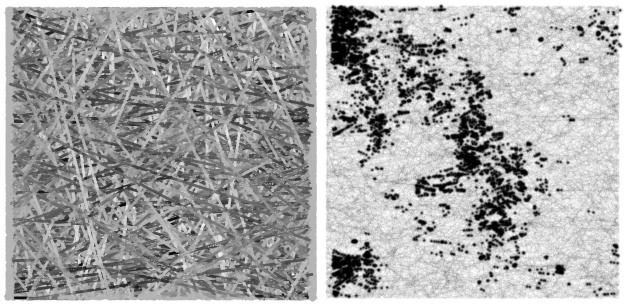

Figure 3.3: In the left figure are strains resulting in a tensile stiffness simulation, and in the right figure there is a dot on each edge broken in a strength simulation.

Figure 3.4: Profile of a bend curve in a bending resistance simulation.

These results are promising, considering the model's simplicity. The linear relation in tensile data and the quadratic relation in the bending data are observable. Moreover, the results are in good agreement, considering the number of properties each model can represent. Altogether, the model generated with justified parameters produces representative results for both tensile stiffness, tensile strength, and bending resistance in cross and machine direction for several different grammages.

The simulations are fast and are performed in minutes. In Figure 3.6 the numerical metrics for a tensile stiffness and tensile strength simulation for each case in the experiment is presented. These execution times are viable for a paper developer who wants to check a hypothesis on consumer-grade hardware.

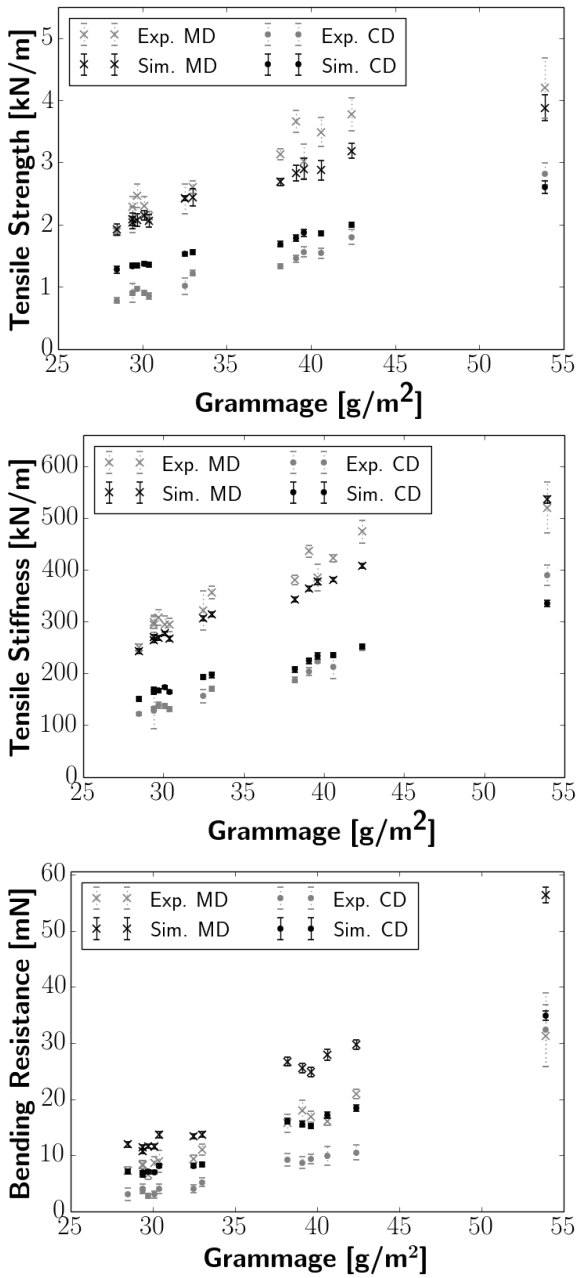

Figure 3.5: Validation results of The Packaging Greenhouse experiments.

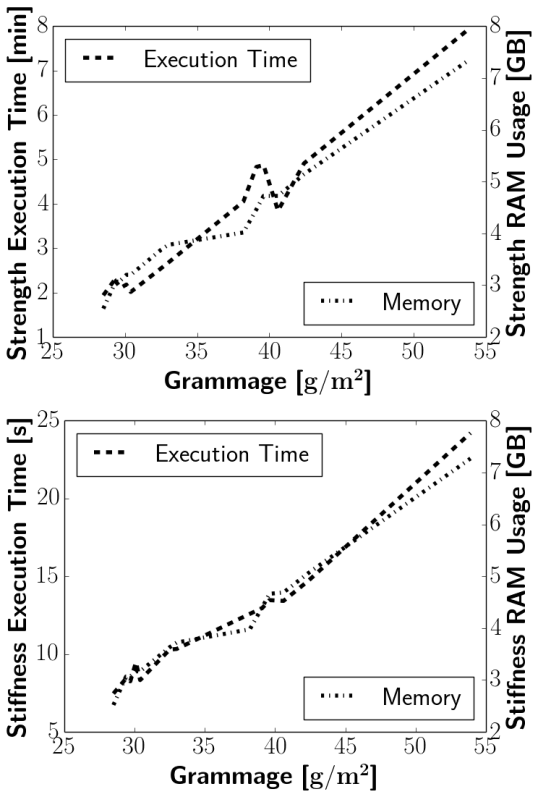

Figure 3.6: The numerical metrics for the mechanical simulations of the Packaging Greenhous experiments.

Stora Enso and Albany experiments, 2020

The second set experiment used for validation is on low-density sheets produced at Albany International on an experimental paper machine, with mechanical properties experiments conducted by Stora Enso. These sheets are almost twice as thick as the Packaging Greenhouse samples. Only tensile stiffness and tensile strength were included in these experiments, not bending resistance, with one experiment performed per property. Similar to The Packaging greenhouse validation, ten different random networks (with the same parameters and fibers as the previous validation) are generated and analyzed for each paper in the experiment. The mean value and standard deviation of the ten simulations for each experiment are presented in Figure 3.7.

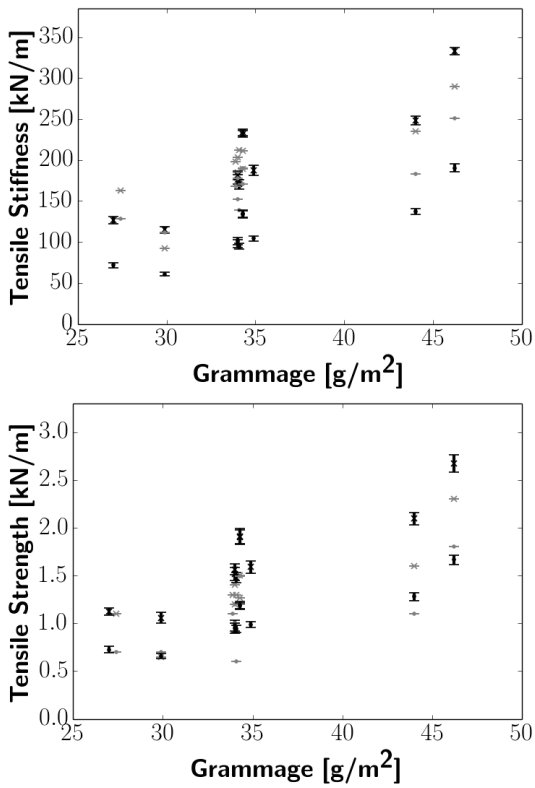

Figure 3.7: Validation results using experiments on low density sheets. Ten random network models were used to simulate each experiment.

The combined results from validating the two sets of experimental data show a model that can correctly anticipate structural properties with justifiable parameters. These results motivate the development of simplified paper models, and due to the effective nature of the model, far denser paper models, such as paperboard, should be possible to simulate. Moreover, as shown in the following chapters, these network models are candidates for a multiscale method. This multiscale method can enable effective large-scale simulations assuming periodic structures on the size analyzed in this section.

CHAPTER 4

Multiscale Methodology for Discrete Network Models

The network model presented in Section 2 constitutes a detailed representation of a paper sheet. These details result in numerical problems requiring excessive resources for small models (see Figure 3.6). Enabling substantially larger simulations than the ones presented in Chapter 3 will require some form of numerical upscaling, for example, a multiscale method.

The multiscale method proposed to handle the large discrete paper models is the Localized Orthogonal Decomposition (LOD) method, a generalization of the finite element method, and is not dependent on periodicity in the model. The original method aimed to handle elliptic partial differential equations with highly varying coefficients [25], and a detailed overview of the method and theory can be found in [13]. In [18], a discrete version of the method was proposed for network models, along with initial numerical results on semi-structured discrete linear elasticity models. This numerical validation was extended to include network models similar to the ones presented in Chapter 2 in **Paper A**. At that point, the application was entirely experimental, and after theoretical development **Paper C**, the implementation has changed slightly. However, numerical experiments show that the new implementation act similarly or better than the old results.

In the following chapter, a discrete LOD method is presented that is motivated by

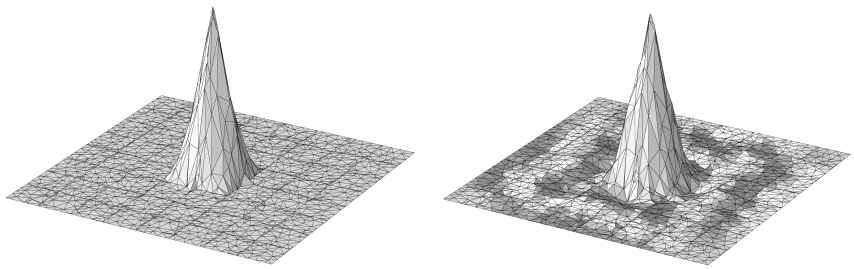

Figure 4.1: The left image shows a bilinear shape function, and the right shows a modified bilinear shape function used in an LOD method.

the theoretical foundation laid out in **Paper C**. First, an overview of the LOD method is presented, followed by some theoretical background and assumptions on the networks considered. Then the scope of problems covered by the theory is defined. With the network and problems specified, the coarse grid of the model is constructed. This chapter ends with formulating an ideal multiscale method and the LOD method with associated a priori error bounds.

4.1 Overview of the LOD method

The localized orthogonal decomposition (LOD) method is a generalized finite element method. A coarse grid represents a model's initial geometry as in a classic finite element method, and a set of shape functions is defined on the grid's points. These shape functions should be able to represent the solution. The shape functions are often smooth and require the grid to be fine enough to handle any potential heterogeneities. For inherently heterogeneous models, this approach is insufficient, and the LOD method solves this issue by resolving the heterogeneities into the basis functions. A triangulation of a discrete bilinear basis function and triangulation of a discrete bilinear basis function used in a LOD method can be found in Figure 4.1.

The heterogeneities must be handled locally for the LOD method to be computationally feasible. In **Paper A** it was numerically confirmed for network models, and in **Paper C** it was proven. The method is feasible but not faster. The method is slower than using a standard linear solver to solve an individual problem. However, memory constraints are an issue for large problems (where off-the-shelf iterative methods have convergence issues). These memory issues are not a problem for

the LOD method, which breaks the problem into smaller local subproblems. The method may be faster in iterative processes, like fracture propagation, where most modifications are identical between iterations. Another motivator would be the use of periodic models. If the model is periodic, embeddings will be periodic, and hence only a fraction of the modified shape functions need to be computed.

4.2 Theoretical foundation

Before anything, we define what we mean by a spatial network, some fundamental network properties, important funciton spaces, and network related operators.

Definition 1 (Spatial network)**:** *A spatial network, $\mathcal{G} = (\mathcal{N}, \mathcal{E})$, is defined by a finite nodal set $\mathcal{N} = \{x_1, x_2, \ldots\}$, $x_i \in \mathcal{R}^d$, $i = 1, \ldots$, and an edge set $\mathcal{E} \subset \{\{n_1 \in \mathcal{N}, n_2 \in \mathcal{N}\} : n_1 \neq n_2\}$, where d is the spatial dimention of the network. An element in the nodal set $\mathcal{N}$ is called a node and these nodes are connected by edges that are defined by the unordered pairs in the edge set $\mathcal{E}$. The notation $i \sim j$ is used to say that $x_i, x_j \in \mathcal{E}$.*

The edges in these spatial networks can be seen as paths, or connections, between the nodes. These edges might represent springs or beams in a structural network, and in a logistic network, the edges might represent routs between transit points. Considering the logistic example, whether a path exists between two transit points is important. This property will be essential in the following discussion, so a formal definition of a path and connected network is formalized.

Definition 2 (Path)**:** *Let $\{z_l\}_{l=1}^m$ be a sequence of nodes from the node set of a network. Then we call the sequence $\{\{z_k, z_{k+1}\}\}_{k=1}^{m-1}$ a path from node x_i to x_j if $z_1 = x_i$, $z_1 \sim z_2$, $z_2 \sim z_3$, $\ldots, z_{m-1} \sim z_m$, and $z_m = x_j$.*

Definition 3 (Connected Network)**:** *A spatial network $\mathcal{G} = (\mathcal{N}, \mathcal{E})$ is connected if for any two distinct nodes $x_i, x_j \in \mathcal{N}$, there exists path between them.*

Definition 4 (Edge length)**:** *The edge length of an edge, $\{x_i, x_j\} \in \mathcal{E}$, in a spatial network is defined by the euclidian distance, $|x_i - x_j|$, between the two nodes in the node pair.*

The following restrictions on the network models considered are imposed:

Assumption 1:

- *The nodes in the nodal set reside in the unit cube* $[0,1]^d$.
- *Every edge in the network has a non zero length.*
- *The network is connected*

The first assumption is imposed for notational brevity, where rectangular domains are also covered, and polygonal domains should be possible with future work. The second assumption guarantees that the lengths of the edges are non-vanishing, which will be important in following network operators. For the third and final assumption, the network needs to be connected. If the network is disconnected, the problems induced by the network model are either separable or attain no solution. This assumption can be imposed by either removing the disconnected components or breaking the problem into several smaller ones.

With the network model defined, we define the function space $\hat{V}$ as the set of real-valued functions defined for each node in $\mathcal{N}$. Note, the spatial network considered induces this space. With this function space, we introduce the linear operator $M : \hat{V} \to \hat{V}$, and the linear operator $L : \hat{V} \to \hat{V}$:

Definition 5:

$$(Mu,v) = \sum_{x_i \in \mathcal{N}} (M_i u, v), \;\; (M_i u, v) = \frac{1}{2} \sum_{i \sim j} |x_i - x_j| u(x_i) v(x_i).$$

Definition 6:

$$(Lu,v) = \sum_{x_i \in \mathcal{N}} (L_i u, v), \;\; (L_i u, v) = \frac{1}{2} \sum_{i \sim j} \frac{(u(x_i) - u(x_j))(v(x_i) - v(x_j))}{|x_i - x_j|}.$$

From these two definitions we can derive the M-norm: $|u|_M^2 = (Mu,u)$ ($\mathcal{G}$ connected, edge lengths are non zero), and the L semi-norm $|u|_L^2 = (Lu,u)$. Moreover, local versions of these norms need to be defined. For compactness, we define the set function N that maps a set in $\mathbb{R}^d$ to the node indecies contained in that set, i.e:

Definition 7:

$$N(\omega) = \left\{ i : x_i \in \mathcal{N},\, x_i \in \omega \right\}.$$

Using this definition our local operators can be defined as $(M_\omega u, v) = \sum_{i \in N(\omega)} (M_i u, v)$, $|u|_{M(\omega)}^2 = (M_\omega u, u)$, where the local counterparts of L are defined annalogoulosly.

The models considered maps information to and from the same data space. This data space can be scalar or vector-valued. In a heat conductivity, the data might be temperature (scalar), and in the structural model presented in Chapter 2 the data is either a displacement or a force (vector-valued). To handle the vector-valued case, we introduce the product space of all possible data

$$\hat{\mathbf{V}} = \hat{V}^n,$$

where n is the dimension of the data for each node.

A function of this space, $\mathbf{v} \in \mathbf{V}$, is written as a list of its components: $\mathbf{v} = [v_{(1)}, \ldots, v_{(n)}]$. Two vector valued operators that will be used are the following vector valued counterparts of L and M:

$$\begin{aligned} \mathbf{M}_i\mathbf{v} &= [M_i v_{(1)}, \ldots, M_i v_{(n)}] \\ \mathbf{L}_i\mathbf{v} &= [L_i v_{(1)}, \ldots, L_i v_{(n)}], \end{aligned} \tag{4.1}$$

where domain restrictions are denoted as in the scalar case. Vector valued semi-norm equivalents are defined:

$$|\mathbf{v}|_{\mathbf{M}}^2 = (\mathbf{M}\mathbf{v}, \mathbf{v}),\ |\mathbf{v}|_{\mathbf{L}}^2 = (\mathbf{L}\mathbf{v}, \mathbf{v}),\ (\mathbf{u}, \mathbf{v}) = \sum_{i=1}^{n} (u_{(i)}, v_{(i)}), \tag{4.2}$$

again with spatial restrictions denoted as in the scalar case.

4.3 Model formulation

The problems considered are spatial network models paired with a linear operator, $\mathbf{K} : \hat{\mathbf{V}} \to \hat{\mathbf{V}}$, and written on the following form:

$$\begin{cases} \mathbf{K}\mathbf{u} = \mathbf{M}\mathbf{f} \\ \mathbf{u}(\Gamma) = 0 \end{cases} \tag{4.3}$$

where Γ is the Dirichlet boundary and $\mathbf{f}$ is a given right-hand side data. This Dirichlet boundary does not need to be the same for each solution dimension for the theory to work, the simplification is made to ease notation. With this, we define the scalar-valued solution space

$$V = \{v \in \hat{V} : v(\Gamma) = 0\},$$

and the vector-valued solution space

$$\mathbf{V} = V^n.$$

The problem homogenized is the weak formulation of (4.3):

$$\text{Find } \mathbf{u} \in \mathbf{V} : (\mathbf{Ku}, \mathbf{v}) = (\mathbf{Mf}, \mathbf{v}),\ \forall \mathbf{v} \in \mathbf{V}. \tag{4.4}$$

The operator $\mathbf{K}$ in the problem is assumed to have the following properties:

Assumption 2: *The operator* $\mathbf{K}$

- *is bounded and coercive on* $\mathbf{V}$ *with respect to* $\mathbf{L}$*, i.e. there are constants* $\alpha > 0$ *and* $\beta \leq \infty$ *such that*

$$\alpha(\mathbf{Lv}, \mathbf{v}) \leq (\mathbf{Kv}, \mathbf{v}) \leq \beta(\mathbf{Lv}, \mathbf{v}) \tag{4.5}$$

  for all $\mathbf{v} \in \mathbf{V}$*, and*
- *can be written as a sum* $\mathbf{K} = \sum_{i \in N} \mathbf{K}_i$ *of operators* $\mathbf{K}_i : \hat{\mathbf{V}} \to \hat{\mathbf{V}}$*, where* $\mathbf{K}_i$ *are symmetric positive semi-definite and only depends and has support on* x_i *and nodes adjacent to* x_i*.*
- *has a null space such that* $\ker(\mathbf{K}) \cap \mathbf{V} = \varnothing$*, to guarantee a unique solution.*

A direct consequence of these assumptions is that $\mathbf{K}$ is symmetric and that $(\mathbf{K}\cdot, \cdot) = (\cdot, \cdot)_K$ is an inner product on $\mathbf{V}$. With this inner product, we introduce the problem-specific semi-norm $|u|^2_{\mathbf{K}} = (u,u)_{\mathbf{K}}$. Local versions of the $\mathbf{K}$ operator and norms are defined the same way using the $\mathbf{K}_i$ operators as the local versions of M and L.

4.4 Coarse scale

The LOD method constructs an accurate course scale representation of the model. This representation is a Galerkin formulation similar to a finite element construction. Neither the network nor the problem is assumed to conform to this construction.

Before we introduce the coarse-scale construction, we first impose three assumptions on the network. These assumptions will guarantee sufficient homogeneity, connectivity, and locality required for the theory. These conditions are constructed using the following boxes:

$$\tilde{B}_R(x) = [x_1 - R, x_1 + R) \times \cdots \times [x_d - R, x_d + R)$$

and

$$B_R(x) = \tilde{B}_R(x) \cup (\overline{\tilde{B}_R(x)} \cap \partial\Omega).$$

Using these boxes, we formulate the following network assumptions.

Assumption 3 (Network assumptions)**:** *There is a length-scale R_0, a uniformity constant σ, density ρ, and a connectivity constant μ, so that*

1. *(homogeneity) for all $R \geq R_0$ and $x \in \Omega$, it holds that*

$$\rho \leq (2R)^{-d} |1|^2_{M,B_R(x)} \leq \sigma\rho,$$

2. *(connectivity) for all $R \geq R_0$, $x \in \Omega$, and $v \in \hat{V}$, it holds that*

$$|v - c|_{M,B_R(x)} \leq \mu R |v|_{L,B_{R+R_0}(x)}$$

   for some constant function $c = c(R,x,v) \in \hat{V}$,
3. *(locality) the edge length $|x_i - x_j| < R_0$ for all edges $\{x_i, x_j\} \in \mathcal{E}$.*

The homogeneity assumption requires that the network's density, in terms of the M norm, is sufficient, the second assumption guarantees connectivity in terms of a discrete poincaré-type inequality, and the third guarantees locality by restricting the geometric range of which the $\mathbf{K}_i$ terms have an effect. For a further discussion and example of the first two assumptions, and how the second assumption is connected the network's Fiedler number [26] and Cheeger constant [27], [28], see **Paper C**.

Like a finite element method, a grid is defined. The grid used is the partition of uniform hypercubes with side length $H = 1/2, 1/4, \ldots$ of Ω:

$$\mathcal{T}_H = \{B_{H/2}(x) : x = (x_1, \ldots, x_d) \in \Omega \text{ and } H^{-1}x_i + 1/2 \text{ are integers for } i = 1, \ldots, d\},$$

where the use of B_R guarantees that $\mathcal{T}_H$ is a true partition of Ω. To guarantee the model has sufficient coverage and connectivity in each partition, we require that:

$$H \geq 4R_0.$$

On this grid, we also define a standard first-order function space. This space, $\hat{Q}_H$, is the union of all element spaces, $\hat{Q}_H(T)$, $T \in \mathcal{T}$, that can be written as the product of componentwise first-order polynomials, i.e,

$$\hat{Q}_H(T) = \{p : p(z_1, \ldots, z_d) = p_1(z_1)p_2(z_2)\cdots p_d(z_2)), p_i \in P_1 \text{ for all } i\}$$

Moreover, we set Q_H and $Q_H(T)$ to be the subspaces of $\hat{Q}_H$ and $\hat{Q}(T)_H$ that are zero on the Dirichlet boundary.

For brevity, we will assume that H is fixed and will ommit notation for components of discrete spaces.

Let $\phi_1, \phi_2, \ldots, \phi_m \in \hat{Q}_H$ be the Lagrangian finite element nodal basis of $\hat{Q}_H$. We order the indecies such that the first m_0 nodal functions are not on the Dirichlet boundary, and therefore span Q_H.

Discrete versions of all these components need to be defined. We denote the restrictions of $\hat{Q}_H$, Q_H, and $\hat{Q}_H(T)$ to the nodal set $\mathcal{N}$ as $\hat{V}_H$, V_H, and $\hat{V}_H(T)$ respectively. The nodal basis $\{\phi_1, \phi_2, \ldots, \phi_m\}$ is discretized as well, where φ_i is the restriction of ϕ_i to the nodal set for every i.

With the discrete finite element space defined, we can construct an interpolation operator that takes the network into account. This interpolant is inspired by the Scott-Zhang interpolant [29] and will be the interpolant used to define the multiscale space in the LOD method.

Definition 8 (Interpolant)**:**

$$I(v) = \sum_{k=1}^{m_0} (M_{T_k} \psi_k, v),$$

where T_k is the element that contains the nodal point k and $\psi_k \in \hat{V}_H(T_k)$ has the property:

$$(M_{T_k} \varphi_k, \varphi_l) = \delta_{kl},\ l = 1, \ldots, m.$$

4.5 Numerical homogenizaiton

Taking a classical finite element approach, $\mathbf{u}$ in (4.4) can be approximated by approximating $\mathbf{V}$ by a finite dimensional space. One such example would be:

$$\mathbf{V}_H = \left\{ \mathbf{v} \in \mathbf{V} : \mathbf{v}_{(i)} \in V_H,\ \forall i = 1, \ldots, n \right\},$$

where the FEM-like approximation $\mathbf{u}_H^{\text{FEM}}$ would be:

$$\text{Find } \mathbf{u}_H^{\text{FEM}} \in \mathbf{V}_H :\ (\mathbf{K}\mathbf{u}_H^{\text{FEM}}, \mathbf{v}) = (\mathbf{M}\mathbf{f}, \mathbf{v}),\ \forall \mathbf{v} \in \mathbf{V}_H. \tag{4.6}$$

This approach could work as long as the heterogeneity are resolved by the coarse grid. However, in the paper models presented in Chapter 2 the model is hetroge-

nous throughout. To deal with this problem, the LOD method aims to find a more approriate discrete space to deal with these heterogeneity.

The ideal multiscale method

In a multiscale formulation, we seperate the model into different scales. For this approach, two scales are considered, a representative coarse scale and the complemental fine scale space. The interpolation operator defined in Definition 8 define this fine scale space:

$$\begin{aligned} \mathbf{W} = \ker(\mathbf{I}_H) = \{\mathbf{v} \in \mathbf{V} : \mathbf{I}_H(\mathbf{v}) = \mathbf{0}\}, \\ \mathbf{I}_H(\mathbf{v}) = [I_H(v_{(1)}), \ldots, I_H(v_{(d_s)})] \end{aligned} \tag{4.7}$$

With the coarse scale, $\mathbf{V}_H^{\text{ms}}$, defined as the orthogonal compliment to $\mathbf{W}$ with respect to the inner product induced by $\mathbf{K}$, i.e,

$$\mathbf{V}_H^{\text{ms}} = \{\mathbf{v} \in \mathbf{V} : (\mathbf{K}\mathbf{v}, \mathbf{w}) = 0, \ \forall \mathbf{w} \in \mathbf{W}\}.$$

This coarse space, $\mathbf{V}_H^{\text{ms}}$, has the same dimension as $\mathbf{V}_H$, and the ideal multiscale approximation, $\mathbf{u}_H^{\text{ms}}$ is formulated as:

$$\text{Find } \mathbf{u}_H^{\text{ms}} \in \mathbf{V}_H^{ms} : \ (\mathbf{K}\mathbf{u}_H^{\text{ms}}, \mathbf{v}) = (\mathbf{M}\mathbf{f}, \mathbf{v}), \ \forall \mathbf{v} \in \mathbf{V}_H^{\text{ms}}. \tag{4.8}$$

The following a priori error estimate was proven in **Paper C** under the assumptions presented in this chapter.

Lemma 1: *The error in the approximate solution $\mathbf{u}_H$, defined in equation (4.8), fulfills*

$$|\mathbf{u} - \mathbf{u}_H|_{\mathbf{K}} \leq C_{\mu,\sigma,\alpha} H |\mathbf{f}|_{\mathbf{M}},$$

where $C_{\mu,\sigma,\alpha}$ denotes a dependence on the constants μ, σ, and α from Assumptions 3 and 2.

The LOD method

The ideal multiscale approximation, $\mathbf{u}_H^{\text{ms}}$, is accurate, however finding $\mathbf{u}_H^{\text{ms}}$ is a harder problem than solving the original problem. The difficulty of the ideal method lies in finding a basis for the multiscale space $\mathbf{V}_H^{\text{ms}}$.

A basis for $\mathbf{V}_H^{\text{ms}}$, can be found by using projections. Let $\mathbf{Q} : \mathbf{V} \to \mathbf{W}$ be the fine

scale projection operator defined by:

$$(\mathbf{KQv}, \mathbf{w}) = (\mathbf{Kv}, \mathbf{w}),\ \forall \mathbf{w} \in \mathbf{W},\ \forall \mathbf{v} \in \mathbf{V}. \tag{4.9}$$

Then an alternative way of defining $\mathbf{V}_H^{\text{ms}}$ would then be:

$$\mathbf{V}_H^{\text{ms}} = \{(1-\mathbf{Q})\mathbf{v} :\ \mathbf{v} \in \mathbf{V}\},$$

with any vector $\mathbf{v} \in \mathbf{V}$ having the unique decomposition

$$\mathbf{v} = (\mathbf{v} - \mathbf{Qv}) + \mathbf{Qv} \in \mathbf{V}_H^{ms} \oplus \mathbf{W}.$$

A basis of $\mathbf{V}_H^{ms}$ can be constructed by taking a basis for $\mathbf{V}_H$, $\{\varphi_i\}_i^{nm_0}$, and applying $(1-\mathbf{Q})$ to each basis function. The choice of $\mathbf{V}_H$ is sufficient because the interpolation operator $\mathbf{I}$ is idempotent under $\mathbf{V}_H$ by construction. The computational difficulties reside in calculating the correction term $-\mathbf{Qv}$, as it requires a global system to be solved. However, under the right circumstances $-\mathbf{Qv}$ can be approximated by local computations.

Before we introduce the localization, we decompose the projection operators elementwise. The projection operator $\mathbf{Q}$ can be written as $\mathbf{Q} = \sum_{T\in\mathcal{T}} \mathbf{Q}_T$, where $\mathbf{Q}_T : \mathbf{V} \to \mathbf{W}$ satisfies:

$$(\mathbf{KQ}_T\mathbf{v}, \mathbf{w}) = (\mathbf{K}_T\mathbf{v}, \mathbf{w}),\ \forall \mathbf{w} \in \mathbf{W},\ \forall \mathbf{v} \in \mathbf{V},$$

because $\mathbf{K} = \sum_{T\in\mathcal{T}} \mathbf{K}_T$.

For the method to be computationaly viable, these operators needs to be evaluated locally around each element. This local computational area we call a patch, and is defined using the set funciton $U : \Omega \to \Omega$:

$$U(\omega) := \{x \in \Omega : \exists T \in \mathcal{T}_H : x \in T, \overline{T} \cap \overline{\omega} \neq \varnothing\},\ \text{and}\ U_k(\omega) = U(U_{k-1}(\omega)).$$

An illustration of T, $U(T)$, and $U_2(T)$ is provided in Figure 4.2.

The LOD method approximates $\mathbf{Q}_T$ by only considering components in the patch $U_k(T)$, where k is a localization paramter, by solving:

$$\begin{aligned}(\mathbf{KQ}_T^k\mathbf{v}, \mathbf{w}) &= (\mathbf{K}_T\mathbf{v}, \mathbf{w}),\ \forall \mathbf{w} \in \mathbf{W}(U_k(T)),\\ \mathbf{W}(\omega) &= \{\mathbf{w} \in \mathbf{W} :\ \mathbf{w}(x_i) = 0, \forall i \in N(\omega)\}.\end{aligned} \tag{4.10}$$

These problems can be solved locally for every $\mathbf{v} \in \mathbf{V}$. This approximation is accurate, and in **Paper C** it is proven to have the following exponential convergence with

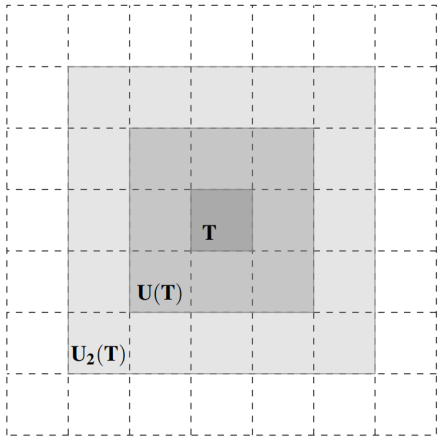

Figure 4.2: An illustration showing the growth of recursive use of the U operator.

respect to k:

Lemma 2: *Under the assumptions presented in this chapter, and $H \geq 4R_0$, we have that for any $\mathbf{v} \in \mathbf{V}$ it holds:*

$$|(\mathbf{Q}_T - \mathbf{Q}_T^k)\mathbf{v}|_{\mathbf{K}} \leq C_{\mu,\sigma,\alpha,\beta} \exp(-kC)|\mathbf{v}|_{\mathbf{K},T},$$

for constants $C_{\mu,\sigma,\alpha,\beta}$ and C.

The global projection operator $\mathbf{Q}_H$ is approximated by $\mathbf{Q}_H^k = \sum_{T\in\mathcal{T}} \mathbf{Q}_T^k$, that only require local compuations. This approximate projection operator is used to approximate the ideal multiscale space, $\mathbf{V}_H^{\text{ms}}$, by:

$$\mathbf{V}_H^{\text{ms},k} = \{(1-\mathbf{Q}^{\mathbf{k}})\mathbf{v} : \ \mathbf{v} \in \mathbf{V}\}.$$

The LOD approximation, $u_H^{\mathrm{ms},k}$, is found by solving the following variational problem:

$$\text{Find } \mathbf{u}_H^{\mathrm{ms},k} \in \mathbf{V}_H^{ms,k} : \ (\mathbf{K}\mathbf{u}_H^{\mathrm{ms},k}, \mathbf{v}) = (\mathbf{M}\mathbf{f}, \mathbf{v}), \ \forall \mathbf{v} \in \mathbf{V}_H^{\mathrm{ms},k}. \tag{4.11}$$

With the main result of paper **Paper C** being the proof of the following a priori error estimate.

Theorem 1: *Under the assumptions presented in this chapter, and* $H \geq 4R_0$*, the error in the approximate solution* $\mathbf{u}_H^k$*, defined in equation (4.11), fulfills*

$$|\mathbf{u} - \mathbf{u}_H^k|_{\mathbf{K}} \leq C_{\mu,\sigma,\alpha,\beta} \left(H + \exp(-kC)\right) |\mathbf{f}|_{\mathbf{M}}.$$

CHAPTER 5

Numerical Upscaling of Network Models

Following the theory presented in Chapter 4, several numerical examples are presented. The first three examples are the ones presented in **Paper C**. These examples are used to verify the theoretical results, both the H convergence and the k convergence of the LOD method. In these examples, both scalar and vector-valued problems are analyzed.

The fourth and final example is one of the validation simulations in Chapter 3, with the simulations redone using a LOD method. In the theoretical results developed in **Paper C**, the network model is assumed to take the form of a unit cube. The network models are thin three-dimensional objects. However, the choice of the domain was more for notational purposes, and initial numerical results indicate that the LOD method can handle these models, with the multiscale approximation able to recreate the tensile properties down to less than one percent with a high degree of localization.

For implementation ideas and pointers on how to create an optimal LOD method, see [30].

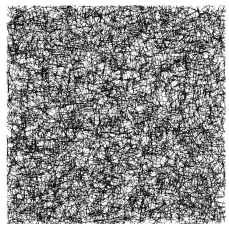

Figure 5.1: The random network model used to validate the theoretical results in **Paper C**.

5.1 A random fiber model

In **Paper C** several numerical examples are presented on a random two-dimensional fiber network. The network was constructed by placing fibers randomly in the unit square with a specified density and fiber length, with the assumptions presented in Chapter 4 numerically confirmed. An illustration of the network is presented in Figure 5.1

Diffusion problem

In the first example, a diffusion problem is upscaled. The problem is based on the $\mathbf{L}$ operator presented in the previous chapter, where the components, $\mathbf{L_i}$ are weighted with random weights between 0.1 and 1. The problem in question has a zero Dirichlet boundary on the entire domain and constant right-hand side data $\mathbf{f} = \mathbf{1}$.

The problem was solved using a linear solver, and that solution is used as a reference solution. This reference solution is compared to the finite element inspired approximation in (4.6) and the LOD approximation (4.11) with localization parameter $k = 2$. The solution to the problem, along with the convergence results for the two approximations with respect to H, is presented in Figure 5.2.

The numerical results clearly indicate that the finite element inspired method is insufficient. The relative error stagnates into a convergence plateau. However, where the first approximation stagnates, the LOD approximations attain the theoretical H convergence in the $\mathbf{K}$-norm. The LOD approximation also has H^2 convergence in the $\mathbf{M}$-norm, which is consistent with an optimal first-order finite element method.

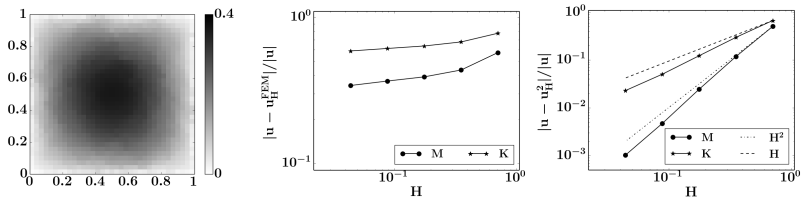

Figure 5.2: The solution of the diffusion problem, along with the convergence results for the finite element and LOD approximation.

Explanation	Parameter	Value
Radius of wire	r_w	2.5 mm
Cross-section Area	A	πr_w^2
Young's modulus	E_A, E_B	210GPa
Second moment of area	I	$0.25\pi r_w^4$

Table 5.1: Structural paramters of the wire mesh structural problem

Structural problem

In the vector-valued example in **Paper C**, the governing model presented in Chapter 2 is used. In this specific example, we use node bonds on the intersection points. The model problem is inspired by a steel mesh of wires with a specified radius, with the parameters presented in Table 5.1.

Two structural problems are analyzed. For the first structural simulation, a two-dimensional tensile simulation is evaluated. In this specific problem, the equilibrium is found given a specified strain. Because the right-hand side is zero and the displacement can be resolved precisely, the ideal multiscale approximation attains the correct solution. Meaning the error introduced in the LOD approximation is entirely based on the localization error of the projection operator $\mathbf{Q}^k$. With this in mind, the convergence error in this example is evaluated with respect to k. An illustration of the exact solution to this problem, along with the k convergence results, are presented in Figure 5.3.

The convergence results in Figure 5.3 is consistent with Theorem 1, where exponential convergence is observed with respect to k. Moreover, exceedingly good approximations can be attained for a localization factor of $k = 2$, which illustrates that the LOD method can work with a high degree of localization.

A constant lateral load is applied to the tensile simulation in the second structural

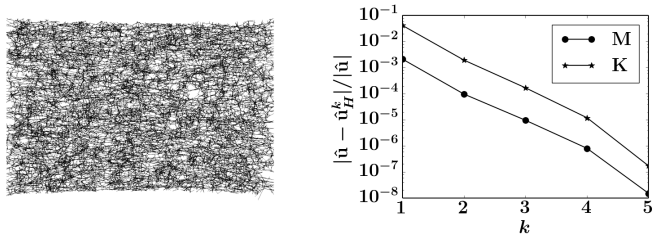

Figure 5.3: The solution of the two-dimensional equilibrium tensile simulation, and the k-convergence results for the LOD approximation.

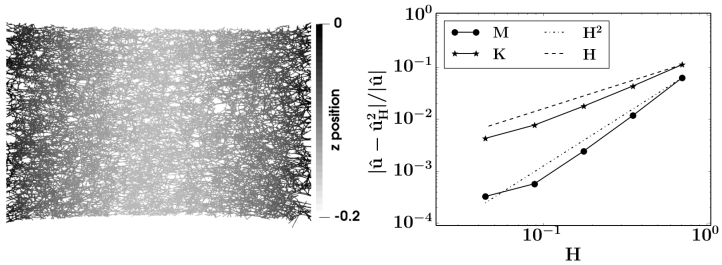

Figure 5.4: The solution of the three dimensional tensile problem with a structural load, and relative errors for the LOD approximation for different H.

problem. This lateral load can be seen as gravity acting on the network, pushing it down. In this problem, the ideal multiscale method does not attain the exact solution, so convergence with respect to H is evaluated. The convergence results for LOD approximations with $k = 2$, and an illustration of the solution is presented in Figure 5.4.

Similar to the previous examples, the theoretical convergence results are consistent with the results in Figure 5.4. We observe a slight stagnation for the last grid analyzed in these results. This stagnation is consistent with the k convergence results in Figure 5.3, which indicates that less localization is required for better results. However, the relative errors of the approximations are less than one percent in the **K**-norm and a tenth of that in the **M**-norm, which is sufficient in most structural simulations.

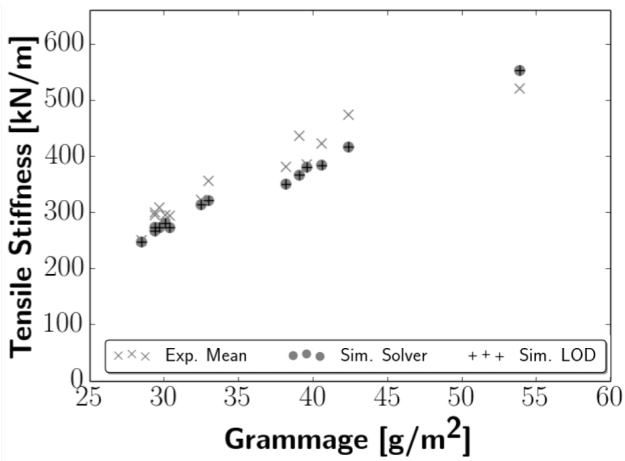

Figure 5.5: The tensile stiffness simulation in cross direction using an LOD solver. **Denna bilden är med gammla resultat, dom nya håller på att köra nu. Bilden kommer dessutom uppdateras så den är enklare att läsa.**

5.2 Validated paper model

The tensile stiffness simulation in the cross direction in Chapter 3 was performed again with a LOD method. Unlike the previous example on the two-dimensional network, the validated paper models are three-dimensional. Each model is exceedingly thin compared to the width of the sheet. This geometric irregularity is resolved by only placing one element in z-direction in the coarse grid and dividing the coarse grid in X-Y direction as in a two-dimensional example. For this particular example, 16×16 elements are used, with localization parameter $k = 2$.

In the numerical experiment, each sheet is only evaluated once, unlike the ten times in the validation. Moreover, nodes are placed on edges that intersect the boundary to reduce boundary effects. With these slight modifications, we produce the results in Figure 5.5 that show that the method produces almost identical results as using a linear solver. Less than one percent difference in the approximation compared to the exact solution for each simulation performed.

CHAPTER 6

Summary and Future Work

This chapter will summarize the content of this book and discuss potential future development.

6.1 Summary

A paper model based on linearized one-dimensional beam theory was presented in Chapter 2. The model is based on the initial work in [17] and was developed further. This development includes shape-based structural parameters, analyzing and motivating parameters with experimental data, more accurate bonding with the volumes of the paper fibers considered, and a new way to represent fiber bonds.

The paper model presented in Chapter 2, was used to simulate and validate structural experiments in Chapter 3. These experiments included tensile stiffness, tensile strength, and bending resistance. These structural experiments were performed and validated both in machine and cross direction. The validation results show that the model can reproduce representative results. Moreover, these simulations are fast, with a tensile type simulation taking seconds and strength simulations a couple of minutes.

The linear systems resulting from fiber-based network models are enormous, and

convergence issues for standard preconditioners have led to non-iterative methods. Even though the simulations with the paper model in Chapter 3 are fast in execution time, they require a decent amount of memory. Simulations on larger domain sizes scale poorly, and to deal with this, numerical upscaling is proposed.

In Chapter 4 the LOD multiscale method is presented. The chapter presents some standard network notation, operators, and discrete functions spaces. These definitions are used to formulate weak connectivity, homogeneity, and locality assumptions on the network and model, with the paper model being covered by these assumptions. Using a synthetic grid that the network does not need to conform to, an interpolation operator is constructed that takes the network into account. This interpolation operator is used to formulate the LOD approximation, and an a priori error bound can be formulated under the earlier assumptions.

The a priori error bound in Chapter 4 is numerically confirmed in Chapter 5. In this chapter, multiple fiber-based numerical examples are presented and analyzed, including a scalar diffusion problem and two structural problems based on the governing model in Chapter 2 on the same two-dimensional network. This two-dimensional network was analyzed in **Paper C**, and the network assumptions on the network model were numerically validated. The numerical results are consistent with the theoretical a priori error bound presented in Chapter 4 and proven in **Paper C**. Chapter 4 ends with performing a tensile stiffness validation simulation from Chapter 3 with the LOD method, matching the validation results with less than one percent difference.

6.2 Future work

This book presents an efficient, thoroughly validated paper model and a mathematically proven multiscale framework for upscaling them. These results provide a solid foundation for further development in several different directions.

The model is efficient and representative. Analyzing higher density sheets like paperboard should still be manageable on smaller domain sizes on consumer hardware. It might be possible to extend the validation results to thicker multi-layer paper with further work. Moreover, thicker paper, such as paperboard, has other structural properties of interest (for example, Z-strength) that would be interesting to evaluate as well. Within the ISOP project, a framework for laydown and paper forming simulations has been developed [5]. Using the geometry from a paper forming simulation as the geometries in a structural simulation would provide a complete framework for a papermaker to analyze the structural effects of paper for different machine settings.

Introducing time dependence in the paper model would be interesting. The tensile stiffness simulations are accurate, and if a more advanced model predicts similar results, the simplified nature of the model would be further justified. In the tensile strength simulations, it might be possible to get accurate stress/strain curves. Our model produces slightly stiffer values in the simulation than in the bending resistance experiment, so it would be interesting to see how bending stiffness differs in a time-dependent version.

An efficient LOD implementation of the strength simulations should be possible. The computational difficulty of solving a stiffness problem might be similar to a strength simulation by only updating the multiscale basis functions where the edges break between iterations. A similar implementation can be used for potential time-dependent implementations of the model, where the multiscale basis functions are only updated under specified circumstances.

If the paper model is periodic on some scale, the LOD method resolves the microscale (fibers) on only one period. The computational complexity will be restricted to the coarse-scale problem by reusing the basis functions for the multiscale space. Simulations as extensive as A4 sheets that take individual paper fibers into account might be possible, using periodicity in the paper model, depending on how the coarse problem scales.

CHAPTER 7

Summary of included papers

This chapter provides a summary of the included papers.

7.1 Paper A

Morgan Görtz, Gustav Kettil, Axel Målqvist, Andreas Mark, Fredrik Edelvik
A numerical multiscale method for fiber networks
Published in WCCM-ECCOMAS 2020 preceedings .

Article summarizing the initial numerical validations of the LOD method on discrete fiber-based network models. The results are an extension of the results presented in [18], showing that the LOD method is capable of upscaling less structured networks. These initial numerical results motivated us to continue the theoretical development of the LOD method's use on general network problems.

7.2 Paper B

Morgan Görtz, Gustav Kettil, Axel Målqvist, Mats Fredlund, Kenneth Wester, Fredrik Edelvik

Network models for predicting structural properties of paper
Submitted to Nordic Pulp and Paper Research Journal. .

In this article, the paper network model presented in Chapter 2 is presented, analyzed, and validated. First, the network model parameters are methodically defined either with experimental data or using published values in literature. The model's discretization parameters are analyzed, with sufficient discretization parameters chosen. Tensile stiffness, tensile strength, and bending resistance experiments are simulated and validated against experimental data in cross- and machine direction. The simulation domains chosen are motivated by domain studies, showing that the forces scale appropriately for different domains sizes. The validation results show that the paper network model can simulate the mentioned structural experiments accurately. Moreover, the simulations are fast, with the simulations only taking a couple of minutes on consumer-grade hardware.

7.3 Paper C

Fredrik Edelvik, Morgan Görtz, Fredrik Hellman, Gustav Kettil, Axel Målqvist
Numerical homogenization of spatial network models
Article draft with the theoretical work so far .

This article presents the mathematical foundation used to prove an a priori error bound for the LOD method on general network problems. The article defines what assumptions are required on the networks and associated problems. These assumptions relate to the network's and model's connectivity, homogeneity, and locality. The paper network model presented in Chapter 2 is covered by the assumptions. These assumptions make it possible to construct an artificial uniform coarse grid and an effective interpolation operator for the LOD method. The main result of this paper is a proven a priori error bound for LOD approximations.

References

[1] M. Hubbe, "Bonding between cellulosic fibers in the absence and presence of dry-strength agents – a review," *Bioresources*, vol. 1, no. 2, 2007.

[2] V. Tojaga, A. Kulachenko, S. Östlund, and T. C. Gasser, "Modeling multi-fracturing fibers in fiber networks using elastoplastic timoshenko beam finite elements with embedded strong discontinuities — formulation and staggered algorithm," English, *Comput. Methods Appl. Mech. Eng.*, vol. 384, 2021.

[3] S. Lavrykov, S. B. Lindström, K. M. Singh, and B. V. Ramarao, "3d network simulations of paper structure," English, *Nord. Pulp. Pap. Res. J.*, vol. 27, no. 2, pp. 256–263, 2012.

[4] H. Askfelt and M. Ristinmaa, "Response of moist paperboard during rapid compression and heating," *Appl. Math. Model.*, vol. 42, pp. 114–132, 2017.

[5] G. Kettil, A. Mark, K. Wester, M. Fredlund, and F. Edelvik, "Numerical investigation of upstream cylinder flow and characterization of forming fabrics," *Nord. Pulp. Pap. Res. J.*, vol. 34, no. 3, pp. 371–393, 2019.

[6] J. Göhl, A. Mark, S. Sasic, and F. Edelvik, "An immersed boundary based dynamic contact angle framework for handling complex surfaces of mixed wettabilities," *Int. J. Multiph. Flow.*, vol. 109, pp. 164–177, 2018.

[7] S. Heyden, "Network modelling for evaluation of mechanical properties of cellulose fibre fluff," Ph.D. dissertation, 2000, ISBN: 91-7874-076-2.

[8] R. Ewing, O. Iliev, R. Lazarov, I. Rybak, and J. Willems, "A simplified method for upscaling composite materials with high contrast of the conductivity," *SIAM J. on Sci. Comput.*, vol. 31, pp. 2568–2586, 2009.

[9] S. Friedland and R. Nabbem, "A distributed model of traffic flows on extended regions," *Netw. Heterog. Media*, vol. 5, pp. 525–544, 2010.

[10] J. Chu, B. Engquist, M. Prodanović, and R. Tsai, "A multiscale method coupling network and continuum models in porous media i: Steady-state single phase flow," *Multiscale Model. Simul.*, vol. 10, pp. 515–549, 2012.

[11] E. Weinan and B. Engquist, "The heterognous multiscale methods," *Commun. Math. Sci.*, vol. 1, pp. 87–132, 2003.

[12] T. Hou and X.-H. Wu, "A multiscale finite element method for elliptic problems in composite materials and porous media," *J. Comput. Phys.*, vol. 134, pp. 169–189, 1997.

[13] A. Målqvist, *Numerical homogenization by localized orthogonal decomposition*. SIAM Spotlights, 2020.

[14] A. Målqvist and A. Persson, "A generalized finite element method for linear thermoelasticity," *ESAIM: Mathematical Modelling and Numerical Analysis*, vol. 51, pp. 1147–1171, 2017.

[15] P. Henning and A. Persson, "A multiscale method for linear elasticity reducing poisson locking," *Comput Methods Appl Mech Eng*, vol. 310, pp. 156–171, 2016.

[16] G. Kettil, "Multiscale methods for simulation of paper making," Ph.D. dissertation, 2019.

[17] A. Kulachenko and T. Uesaka, "Direct simulations of fiber network deformation and failure," *Mech. Mater.*, vol. 51, pp. 1–14, 2012.

[18] G. Kettil, A. Målqvist, A. Mark, M. Fredlund, K. Wester, and F. Edelvik, "Numerical upscaling of discrete network models," *BIT Numer. Math.*, vol. 60, no. 1, pp. 67–92, 2020.

[19] G. Wang, S. Q. Shi, J. Wang, Y. Yu, S. Cao, and H. Cheng, "Tensile properties of four types of individual cellulosic fibers," *Wood Fiber Sci.*, vol. 43, no. 4, pp. 353–364, 2011.

[20] L. H. Groom, L. Mott, and S. Shaler, "Mechanical properties of individual southern pine fibers. part i. determination of variability of stress-strain curves with respect to tree height and juvenility," *Wood Fiber Sci.*, vol. 34, no. 1, pp. 14–27, 2002.

[21] A. R. Horn, "Morphology of wood pulp fiber from softwoods and influence on paper strength," U.S. Department of Agriculture Forest Service, Tech. Rep., 1974.

[22] A. Brandberg, S. Reyier Österling, A. Kulachenko, and U. Hirn, "Characterization and impact of fiber size variability on the mechanical properties of fiber networks with an application to paper materials," *International Journal of Solids and Structures*, vol. 239-240, 2022.

[23] *Prediction of fibre orientation and stiffness distribtuitions in paper - an engineering approach*, (Oxford, UK), Advances in pulp and paper research, Oxford 2009 : transactions of the 14th Fundamental Research Symposium held in Oxford: September 2009, 2009, pp. 1039–1078.

[24] C. Neagu, K. Gamstedt, and F. Berthold, "Stiffness contribution of various wood fibers to composite materials," *J. Compos. Mater.*, vol. 40, no. 8, pp. 663–699, 2006.

[25] A. Målqvist and D. Peterseim, "Localization of elliptic multiscale problems," *Math. Comp.*, vol. 83, pp. 2583–2603, 2014.

[26] M. Fiedler, "Algebraic connectivity of graphs," *Czechoslovak Mathematical Journal*, vol. 23, pp. 298–305, 1973.

[27] J. Cheeger, "A lower bound for the smallest eigenvalue of the laplacian," in *Problems in Analysis*, R. C. Gunning, Ed. Princeton University Press, 2015, pp. 195–200.

[28] S. Friedland and R. Nabbem, "On cheeger-type inequalities for weighted graphs," *J. Graph Theory*, vol. 41, pp. 1–68, 2002.

[29] R. Scott and S. Zhang, "Finite element interpolation of nonsmooth functions satisfying boundary conditions," *Math. Comp.*, vol. 54, pp. 483–493, 1990.

[30] C. Engwer, P. Henning, A. Målqvist, and D. Peterseim, "Efficient implementation of the localized orthogonal decomposition method," *Comput. Methods Appl. Mech. Engrg.*, vol. 350, pp. 123–153, 2019.